The LINC complex is essential for hearing

Henning F. Horn,[1] Zippora Brownstein,[2] Danielle R. Lenz,[2] Shaked Shivatzki,[2] Amiel A. Dror,[2] Orit Dagan-Rosenfeld,[2] Lilach M. Friedman,[2] Kyle J. Roux,[3] Serguei Kozlov,[4] Kuan-Teh Jeang,[5] Moshe Frydman,[2,6] Brian Burke,[1] Colin L. Stewart,[1] and Karen B. Avraham[2]

[1]Institute of Medical Biology, A*STAR, Singapore. [2]Department of Human Molecular Genetics and Biochemistry, Sackler Faculty of Medicine, Tel Aviv University, Tel Aviv, Israel. [3]Sanford Research/USD Children's Health Research Center, Sioux Falls, South Dakota, USA. [4]National Cancer Institute, Frederick, Maryland, USA. [5]Laboratory of Molecular Microbiology, National Institute of Allergy and Infectious Diseases, NIH, Bethesda, Maryland, USA. [6]Danek Gertner Institute for Medical Genetics, Sheba Medical Center, Tel Hashomer, Israel.

Hereditary hearing loss is the most common sensory deficit. We determined that progressive high-frequency hearing loss in 2 families of Iraqi Jewish ancestry was due to homozygosity for the protein truncating mutation *SYNE4* c.228delAT. *SYNE4*, a gene not previously associated with hearing loss, encodes nesprin-4 (NESP4), an outer nuclear membrane (ONM) protein expressed in the hair cells of the inner ear. The truncated NESP4 encoded by the families' mutation did not localize to the ONM. NESP4 and SUN domain–containing protein 1 (SUN1), which localizes to the inner nuclear membrane (INM), are part of the linker of nucleoskeleton and cytoskeleton (LINC) complex in the nuclear envelope. Mice lacking either *Nesp4* or *Sun1* were evaluated for hair cell defects and hearing loss. In both $Nesp4^{-/-}$ and $Sun1^{-/-}$ mice, OHCs formed normally, but degenerated as hearing matured, leading to progressive hearing loss. The nuclei of OHCs from mutant mice failed to maintain their basal localization, potentially affecting cell motility and hence the response to sound. These results demonstrate that the LINC complex is essential for viability and normal morphology of OHCs and suggest that the position of the nucleus in sensory epithelial cells is critical for maintenance of normal hearing.

Introduction

Hereditary hearing loss is the most common sensory deficit that affects as many as 0.1–0.3% of newborns (1). Hearing impairment represents a genetically heterogeneous group of disorders that may either include other clinical symptoms as syndromic hearing loss (SHL) or appear alone as non-syndromic hearing loss (NSHL). Investigations into the molecular basis of NSHL have led to the discovery of both common and rare forms of deafness. To date, mutations in over 60 genes encoding a functionally diverse group of proteins, and at least 1 microRNA, are known to cause NSHL. This number is increasing with the advent of advanced genomic sequencing technologies (2). The genetic heterogeneity of hearing loss reflects the complexity of the human auditory system, which comprises multiple highly specialized cell types, including both inner hair cells (IHCs) and outer hair cells (OHCs) as well as supporting cells and neurons, each with their own unique structural features.

In the vertebrate ear, sound perception is mediated by the cochlea, in essence a coiled liquid-filled tube that receives sound waves from the eardrum via the ossicles in the middle ear (3). Extending the entire length of the cochlea is the organ of Corti, the epithelial cell–based structure that transforms sound waves into electrical impulses that are transmitted to the spiral ganglion and auditory nerve. The IHCs and OHCs are the sensory cells within the organ of Corti, which contain mechano-sensitive stereocilia on their apical surfaces. In mammals, a single row of IHCs and 3 rows of OHCs extend from the base of the cochlea to its apex. The IHCs serve as sensory receptors, being innervated mostly by auditory afferents. The OHCs, with scattered afferent innervation, play a specific role in amplification of sounds based on their motility (4).

The nuclear envelope (NE), as the interface between the nucleus and cytoplasm, displays several major structural features, the most prominent of which are the inner and outer nuclear membranes (INM and ONM) separated by a gap or perinuclear space (PNS) of about 50 nm (5). Although biochemically distinct, the 2 membranes are joined where they are spanned by nuclear pore complexes, the large multi-protein channels mediating nucleo-cytoplasmic trafficking of macromolecules. Lining the nuclear face of the INM is the nuclear lamina, a meshwork of filamentous proteins, the nuclear lamins, which provide the NE with its structural integrity. Nesprin-4 is a member of the KASH (Klarsicht, Anc1, Syne homology) domain family of ONM proteins, originally identified in secretory epithelial cells, and functions as an NE adapter for conventional kinesin-1, a microtubule plus-end motor protein (6). The majority of KASH domain proteins, which are found in all eukaryotes, interact with the actin and intermediate filament cytoskeletal networks, as well as microtubule-dependent motor proteins (7). Localization of KASH proteins to the ONM is dependent upon SUN (Sad1, UNC-84) domain proteins of the INM. SUN domain proteins, from yeast to humans, share a common topology where the N-terminal domain invariably faces the nucleoplasm and interacts with a variety of nuclear components, including members of the nuclear lamin family. SUN-KASH pairs represent so-called LINC complexes (for linker of nucleoskeleton and cytoskeleton), which couple nuclear components to the cytoskeleton (8). Most compelling, a significant number of diseases and anomalies, spanning cardiac and skeletal myopathies, lipodystrophies, peripheral neuropathies, and premature aging with early death, are associated with mutations in proteins of the NE and the lamina (9, 10).

Here, we demonstrate that hearing loss is caused by defects in either of 2 proteins that localize to the nuclear membranes of hair cells: nesprin-4, which localizes to the ONM and Sun1 (SUN domain-containing protein 1), which localizes to the INM. We suggest that abnormal nuclear positioning leads to OHC death either due to interference with their sound-induced motility or to a compromised ability of abnormal OHCs to withstand the mechanical rigors of motility.

Authorship note: Henning F. Horn and Zippora Brownstein are co–first authors.
Conflict of interest: The authors have declared that no conflict of interest exists.
Citation for this article: *J Clin Invest.* doi:10.1172/JCI66911.

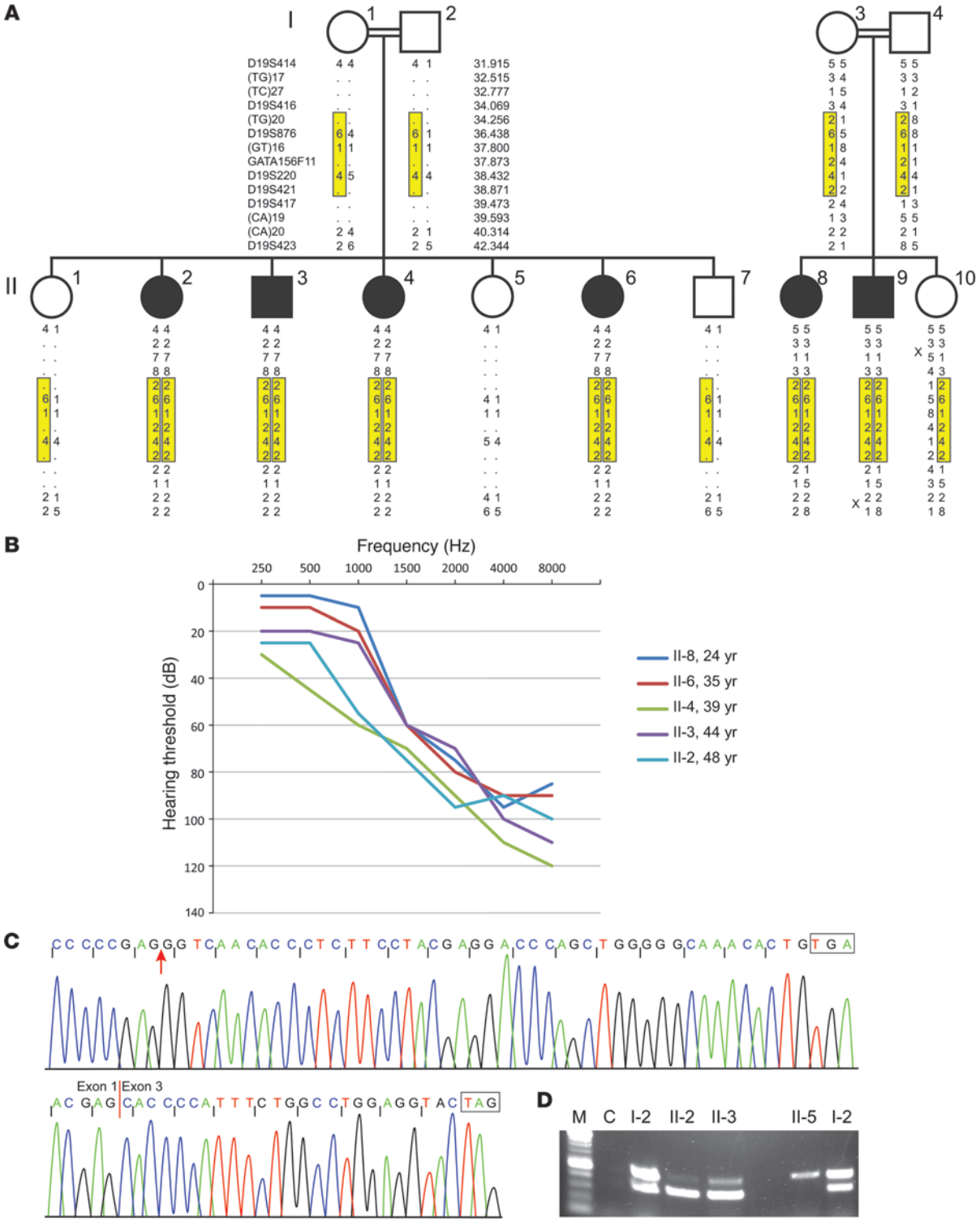

Figure 1

Identification of *SYNE4*, encoding nesprin-4, as a gene responsible for hearing loss. (**A**) Pedigrees of 2 families of Iraqi Jewish origin with hearing loss (black symbols). Hearing loss in the families was mapped by linkage analysis to chromosome 19q, including a 5.4-Mb region homozygous in all affected individuals (highlighted in yellow). (**B**) Audiograms of affected individuals, demonstrating high-frequency hearing loss. (**C**) Sanger sequencing (patient II-3) of the site of the c.228delAT mutation (upper sequence) revealing the deletion of 2 bp and surrounding sequence extending to the new stop codon (W77VfsX16). The bottom Sanger sequence (patient II-3) demonstrates a portion of the mutant transcript, with the deletion of exon 2 (delEx2), showing a part of exon 1 and part of exon 3, until the premature stop codon. (**D**) Amplification of exons 1–4 from cDNA derived from lymphoblasts resulted in a PCR product of 491-bp fragment, whereas skipping of exon 2 resulted in a product of 151-bp in all individuals carrying the c.228delAT mutation.

Results

Identification of SYNE4 as the gene responsible for progressive high-frequency hearing loss in 2 families. Young adults in 2 Israeli families of Iraqi Jewish ancestry presented with a high-frequency hearing impairment (Figure 1, A and B). Hearing loss was first noticed between birth and 6 years and by adulthood had progressed to severe loss at high frequencies. The pattern of hearing loss in the families suggested autosomal recessive inheritance.

We postulated that the distinctive hearing loss phenotype in the 2 families of shared origin might be caused by a single founder allele, homozygous in affected individuals. Microsatellite markers on all chromosomes were first genotyped to map the responsible gene. The single substantial linkage signal was to markers D19S414-D19S220-D19S420 on chromosome 19q with a lod score of 3.2 for the 2 families combined. Additional markers in the linked interval were then genotyped in order to identify a region of homozygosity shared by all 6 affected individuals but not by their hearing siblings. The shared homozygous region is bounded by D19S416 and D19S417, corresponding to the 5.4 Mb genomic interval on chr19: 34,069,009-39,472,484 (hg19) (Figure 1A). The new deafness locus was named DFNB76.

Chromosome 19q13.11-q13.2 is very gene-rich, with more than 100 genes in the critical 5.4-Mb interval. Genes in the interval were Sanger sequenced from genomic DNA of an affected individual from each family and ultimately led to the discovery of a frameshift mutation in *SYNE4* c.228delAT (NM_001039876) at chr19: 36,499,169-36,499,170. As expected, the mutant allele cosegregated with hearing loss in both families. Of 157 hearing controls of Iraqi Jewish ancestry, 4 were heterozygous for the mutation, corresponding to an allele frequency in this community of 0.013. The mutation was not observed in 105 Israeli controls of other origins.

To validate the presence of this mutation and rule out other genes in the region, we used a targeted capture pool we had previously developed for identifying mutations in all known human genes and human orthologs of mouse genes responsible for SHL or NSHL (11). In the current experiment, we added *SYNE4* to a total of 284 human protein-coding genes and microRNAs, of which 163 were the human orthologs of genes associated with the inner ear or deafness in the mouse. No relevant candidates were detected in the SNP and copy-number variation (CNV) analyses. The only candidate recovered in the insertion-deletion (indel) analysis was the AT deletion on chromosome 19, confirming the previously identified mutation.

The *SYNE4* mutation c.228delAT leads to 2 mutant transcripts. The mutation occurs in exon 2 at codon 77 in the 404 amino acid protein (NP_001034965) (Figure 1C). Sequencing of cDNA derived from lymphoblasts yielded 1 mutant transcript with stop 16 codons after the frameshift and a predicted truncated protein of 93 residues (W77VfsX16). The other mutant transcript, 151 bp shorter, skips exon 2 (Figure 1C), leading to a shift in the reading frame and the appearance of a premature stop codon in exon 3, 9 codons downstream of the exon 3 splice junction and yielding a predicted truncated protein of 51 residues. Screening of cDNA derived from lymphoblasts of family members suggests that transcripts lacking WT exon 2 are more abundant (Figure 1D).

Abnormal localization of mutant nesprin-4 proteins. *SYNE4* encodes nesprin-4, a member of the KASH domain family of proteins that localize to the ONM of the NE. Both predicted truncated nesprin-4 proteins lack a coiled-coil and leucine zipper region (residues 102–123), a spectrin repeat (residues 139–201), the kinesin-1–binding region (residues 201–345), and the KASH domain (residues 346–404) (Figure 2A).

Localization of the truncated nesprin-4 proteins was evaluated by comparing WT and mutant proteins following transient expression in COS-7 cells. Western blot analysis of protein extracts from the transfected cells demonstrated the existence of truncated proteins in both of the mutant forms in sizes that correspond to the predicted 51 and 93 amino acid proteins (Figure 2B). Full-length nesprin-4 localizes to the NE, whereas both mutant proteins were found throughout the cytoplasm (Figure 2C).

Hearing loss in Nesp4$^{-/-}$ and Sun1$^{-/-}$ mice. To obtain further insight into the role of nesprin-4 in epithelial cells, we created mice harboring a targeted disruption of the *Nesp4* gene by homologous recombination in ES cells. The gene-targeting strategy resulted in the elimination of part of exon 1 and all of exons 2 through 6 (Figure 3A).

Nesp4$^{-/-}$ mice appear overtly normal with no obvious loss of viability. Nesprin-4 expression was undetectable in salivary gland cells (where nesprin-4 is highly expressed) and the cochlea, as determined by reverse transcriptase PCR (Figure 3B) and Western blot analysis (Figure 3C). Litter size was no different from that of WT animals and the mutant *Nesp4* allele segregated according to Mendelian inheritance patterns. In WT animals, the highest levels of nesprin-4 expression are found in secretory epithelial tissues, including the salivary (Figure 3, B and C) and mammary glands and the exocrine pancreas (6). However, no abnormalities were detected in these tissues following histological analyses (data not shown). Furthermore, weight gain of nursing pups was identical with either WT or *Nesp4*$^{-/-}$ mothers, indicating that there was no significant mammary dysfunction.

Based on the discovery of a human mutation in *SYNE4* linked to autosomal recessive NSHL, hearing in *Nesp4*$^{-/-}$ mice was assessed initially by observation of Preyer's reflex in P30 and P60 mice, revealing a hearing deficit in *Nesp4*$^{-/-}$ animals. Recordings of auditory brainstem response (ABR) confirmed this observation (Figure 3D). Hearing loss of mutant mice was detected already at P15 and progressed to all frequencies by P60. The threshold difference was highly significant ($P < 0.005$) between null and WT mice at all frequencies except at 36 kHz, where $P < 0.05$ was recorded. No significant differences could be detected in heterozygous mice with 1 functional allele of *Nesp4* relative to WT mice. The *Nesp4*$^{-/-}$ mice did not have any circling behavior. More thorough behavioral testing was done, including quantitative analysis of the reaching response and circling and head bobbing, using a modified SHIRPA protocol (12). The mice harbored no abnormal behavior at these levels.

As a member of the KASH-domain protein family, appropriate localization of nesprin-4 to the ONM is dependent upon transluminal interactions with the INM SUN domain proteins. SUN-KASH pairs form the basis of LINC complexes that mechanically couple nuclear and cytoplasmic structures. We reasoned that if hearing loss in *Nesp4* mutant animals was due to compromised LINC complex function, then it might be phenocopied by SUN protein mutations. Both *Sun1*$^{-/-}$ and *Sun2*$^{-/-}$ mice are viable (13–15), with the only documented phenotype in the former being infertility associated with meiotic arrest. *Sun1*$^{-/-}$ and *Sun2*$^{-/-}$ lines were assessed for Preyer's reflex, and a reflex was absent in *Sun1*$^{-/-}$ but not in *Sun2*$^{-/-}$ mice. ABR recordings of *Sun1*$^{-/-}$ mice at P30 revealed a pattern of hearing loss similar to that described for the *Nesp4*$^{-/-}$ animals (Figure 3E).

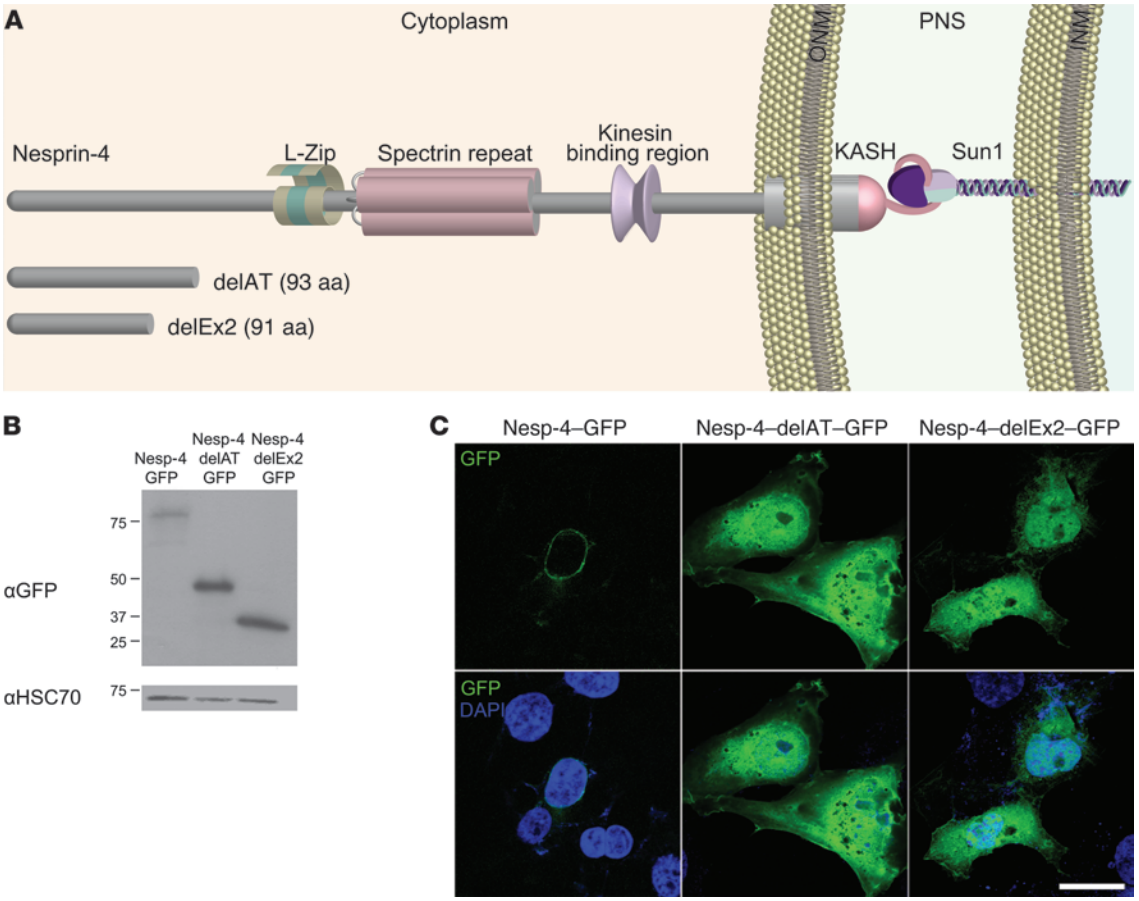

Figure 2
Localization of WT and mutant nesprin-4 proteins. (**A**) Predicted protein scheme of nesprin-4, with putative truncated proteins of 93 (middle) and 51 (bottom) amino acids. (**B**) Western blot analysis of protein extracts from COS-7 cells transfected with GFP-tagged cDNA sequences corresponding to nesprin-4 c.228delAT and lacking exon 2. Staining with anti-GFP reveals truncated proteins from both constructs. Anti-HSC70 served as a loading control. (**C**) Immunofluorescence of transfected cells reveals that while the full-length GFP–Nesp-4 localizes to the ONM as expected, the truncated proteins are localized diffusely throughout the transfected cells. Transfected proteins were visualized via GFP (green), and DAPI was used to stain the nuclei (blue). Scale bar: 20 μm.

Nesprin-4 and Sun-1 are expressed in hair cells of the cochlea. The association between hearing loss and *SYNE4* mutations suggests that nesprin-4 is likely expressed in the inner ear. Quantitative RT-PCR (qRT-PCR) was performed to evaluate expression of RNA in cochleae recovered from mice (Figure 4A). At P0 and P15, the expression was low but rose significantly by P30 ($P < 0.05$) and remained steady. Immunofluorescent staining of whole-mount preparations of cochlear sensory epithelium was performed to evaluate the expression of nesprin-4 and changes in mutant mice. In WT preparations, nesprin-4 was detectable by P0 (data not shown) and at P12 (Figure 4C). Expression was restricted primarily to the 3 rows of OHC and 1 row of IHC of the cochlea. Within the hair cells, nesprin-4 was localized largely to the NE, which appeared as a brightly labeled ring. In other cells of the cochlea, including Deiter's cells and pillar cells, supporting cells of the organ of Corti, nesprin-4 expression was undetectable. There was no detection of nesprin-4 in the hair cells of *Nesp4*$^{-/-}$ mutant mice.

In mammals, Sun1 is widely expressed in somatic and germ cells (13 and 14). Immunofluorescent staining of whole-mount preparations of cochlear sensory epithelium from WT mice localized Sun1 to the NE of OHCs (Figure 4D). If Sun1 is functioning as a tether for nesprin-4 in hair cells' NE, then we would expect to see mislocalization of nesprin-4 in *Sun1*$^{-/-}$ mice. Immunofluorescence analysis of cochleas from the *Sun1*$^{-/-}$ mice did reveal a loss of nesprin-4 from the NE (Figure 4E).

Scanning electron microscopy (SEM) analysis demonstrated that at P0, no differences were observed in the hair cells between *Nesp4*$^{-/-}$ and WT mice (Figure 5A). However, as the mice matured, and after the onset of detectable hearing, the OHCs began to degenerate in a basal to apical gradient, while the IHCs remained intact. Partial degradation of OHCs was seen in the null mice already at the middle turn of the cochlea at P15 but not in the apex. Some degradation was present in the apex as well by P60 (Figure 5A). SEM of the organ of Corti derived from *Sun1*$^{-/-}$ mice revealed comparable degeneration of OHC, but not IHC (Figure 5B).

Loss of nesprin-4 and Sun1 results in abnormal positioning of the nucleus in OHCs. Cochlear OHCs have a distinct morphology, with a columnar appearance and the nucleus positioned at the base of the cell (16). Since OHCs degenerate, we focused on changes in morphology in these cells. Immunofluorescent staining of whole-mount prepara-

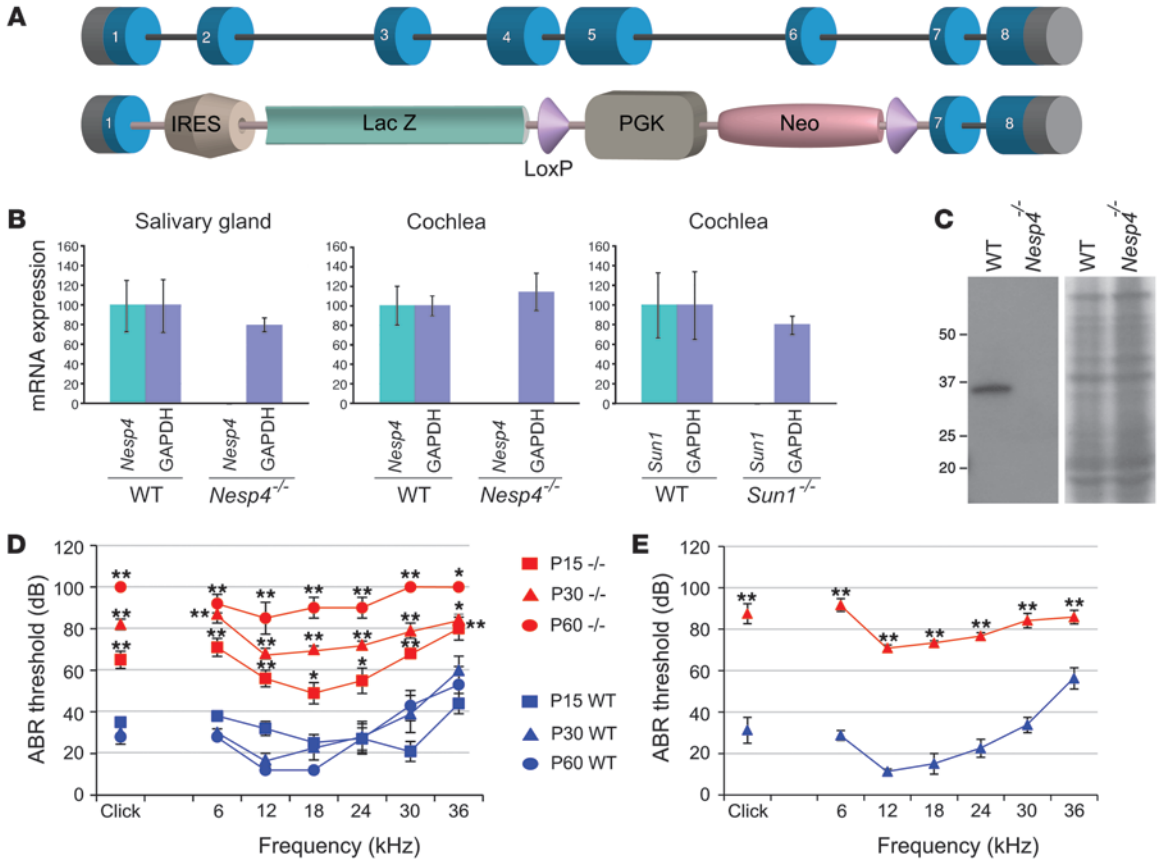

Figure 3

Nesp4 gene-targeted mutagenesis and hearing loss of *Nesp4*$^{-/-}$ mice. (**A**) Schematic representation of the *Nesp4* gene and the KO construct, with an IRES–β-gal cassette inserted instead of exons 2–6 of the *Nesp4* gene. The insertion of the cassette results in an effectively null allele. (**B**) qRT-PCR demonstrated that *Nesp4* mRNA expression is abolished in salivary gland cells and cochlear cells of *Nesp4*$^{-/-}$ mice and *Sun1* mRNA expression is abolished in cochlear cells of *Sun1*$^{-/-}$ mice when compared with similar expression levels of GAPDH. (**C**) Nesprin-4 protein expression is abolished in the *Nesp4*$^{-/-}$ mice, as can be detected by Western blot analysis of salivary gland cells. Coomassie blue staining demonstrates equal loading volumes. (**D**) *Nesp4*$^{-/-}$ mice present with hearing loss, as measured using ABR at ages P15, P30, and P60. Click stimuli were measured in increasing levels, ranging between 10 dB and 90 dB in 5-dB steps, and tone burst stimuli of 6 single frequencies were measured, including 6 kHz, 12 kHz, 18 kHz, 24 kHz, 30 kHz, and 36 kHz in increasing levels between 10 dB and 90 dB in 5-dB steps. ABRs generated from homozygous *Nesp4*$^{-/-}$ mice are shown in red and WT littermates in blue. P15, WT/*Nesp4*$^{-/-}$ n = 5/5; P30, n = 6/5; P45, n = 6/7; P60, n = 5/5. (**E**) *Sun1*$^{-/-}$ mice present with hearing loss, as measured using ABR at age P30. Click and tone burst stimuli were measured as described for *Nesp4*$^{-/-}$ mice. ABRs generated from homozygous *Sun1*$^{-/-}$ mice are shown in red and WT littermates in blue. P30, n = 5/6. Legend applies to parts **D** and **E**. $^{*}P < 0.05$; $^{**}P < 0.005$.

tions of cochlear sensory epithelium revealed a striking difference between *Nesp4*$^{-/-}$ and *Sun1*$^{-/-}$ versus WT OHCs (Figure 6, A and B). Concomitant with the OHC degeneration observed, the nuclei were no longer found at the base of the cells at P14, but were located at the apical region. This aberrant nuclear positioning is observed in all regions of the cochlea that we examined, from the middle region to the apex. In the IHC, the position of the nucleus changes slightly (Figure 6B). These results demonstrate that nesprin-4 and Sun1 play an essential role in the basal positioning of OHC nuclei and at the same time are essential for the maintenance of OHC viability.

Discussion

We describe the involvement of the *SYNE4* gene encoding nesprin-4, an epithelial-specific protein, in hereditary hearing loss in humans. Nesprin-4 is one of 4 nesprins, including nesprins 1–3, that provide binding sites at the nuclear periphery for components of the cytoskeleton. Each of the nesprins possesses a C-terminal KASH domain of 50–60 amino acid residues featuring a transmembrane helix followed by a short luminal sequence. Nesprins are tethered within the ONM by way of transluminal interactions with SUN domain proteins that are residents of the INM (Figure 2A). In mammalian somatic cells, the SUN-domain protein family is represented by Suns 1 and 2. Association between nesprins and Sun1/2 involves the direct interaction of their respective KASH- and SUN-domain sequences within the PNS (17). In this way, nesprins and Sun proteins represent a pair of links in a molecular chain spanning both the INM and ONM, which mechanically couples nuclear structures to the cytoskeleton (6). As we report, nesprin-4 and Sun1 are both expressed in mechanosensory hair cells, where they localize

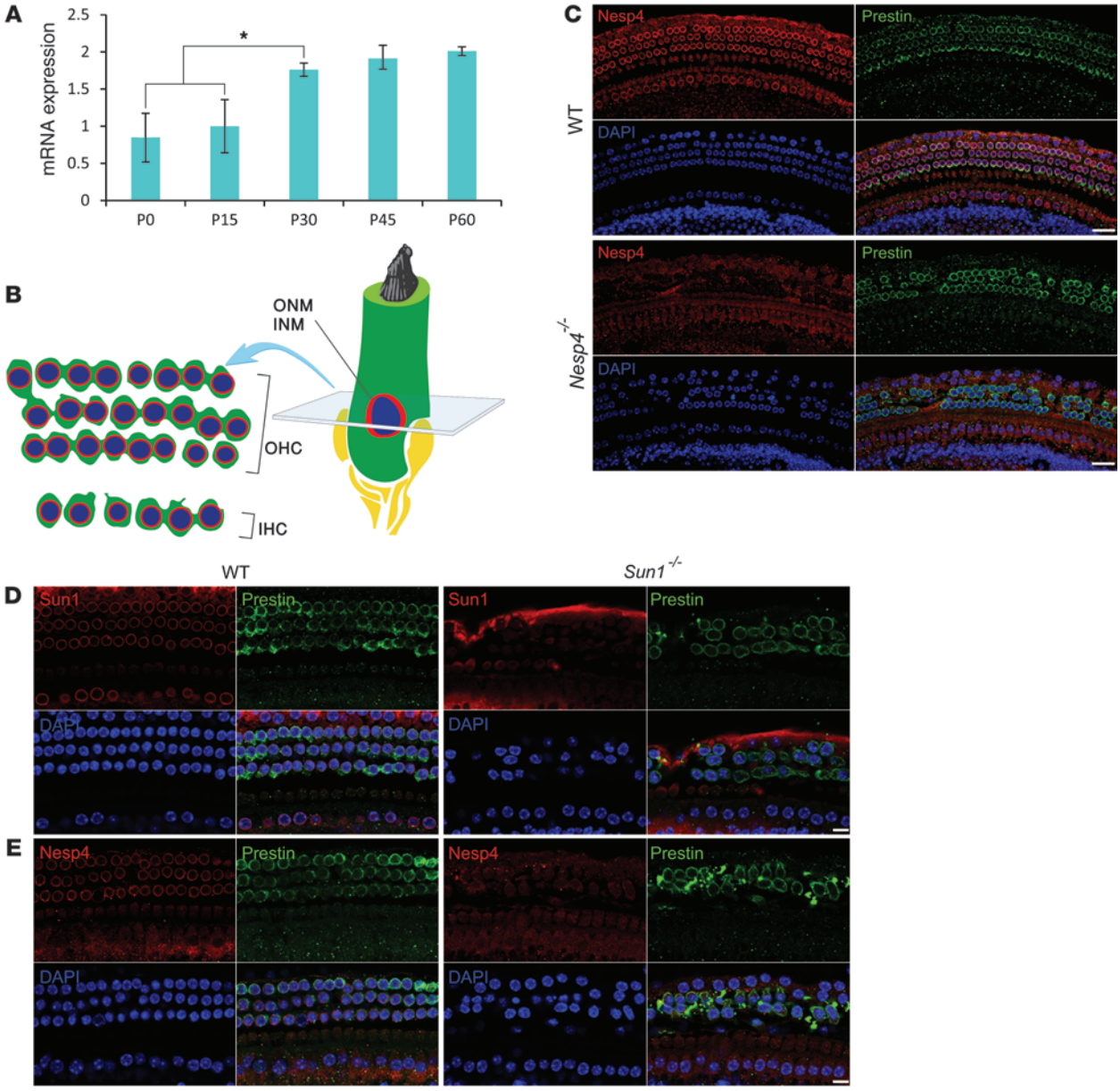

Figure 4

Nesprin-4 and Sun1 are expressed in the cochlea. (**A**) qRT-PCR reveals a gradual increase in *Nesp4* mRNA expression between the ages of P0 and P60. **P* < 0.05. (**B**) Sensory hair cells are embedded within the sensory epithelium along the length of the cochlea. The cell's nucleus is located adjacent to the basal side of the hair cell surrounded by PNS (light green) between the INM and the ONM. A transverse section of cochlear sensory epithelium at the nuclear level reveals the typical arrangement of the sensory cells with 1 row of IHC and 3 rows of OHC. (**C**) Immunofluorescent staining of whole-mount preparations of cochlea derived from P12 WT and *Nesp4*$^{-/-}$ littermate mice. Nesprin-4 is localized to the IHC and OHC of sensory epithelia. Staining for the OHC-specific protein prestin highlights the OHCs. In the *Nesp4*$^{-/-}$ mice, no expression of nesprin-4 was detected, with prestin staining revealing gaps in the rows of OHCs. DAPI (blue) stains the nuclei. (**D**) Immunofluorescent staining of whole-mount preparations of cochlea derived from P25 WT and *Sun1*$^{-/-}$ littermate mice. Sun1 is localized to the IHC and OHC of sensory epithelia. In the *Sun1*$^{-/-}$ mice, no expression of Sun1 was detected, whereas prestin stains the OHC. (**E**) Nuclear membrane localization of nesprin-4 is reduced in OHCs of *Sun1*$^{-/-}$ mice. Scale bars: 15 μm.

primarily to the NE. Thus nesprin-4 and Sun1 likely constitute a hair cell LINC complex isoform that connects the cell nucleus to the cytoskeleton.

A homozygous mutation in the human gene *SYNE4* encoding nesprin-4 leads to progressive high-frequency hearing loss, found in 2 families. Gene-targeted mutagenesis of the mouse *Nesp4* gene led to analogous findings, with hearing loss already detectable at P15 by ABR. Based on the known role of SUN proteins in the tethering of nesprins in the ONM and hence in LINC complex formation, we predicted that mice deficient in Sun1 should display loss of

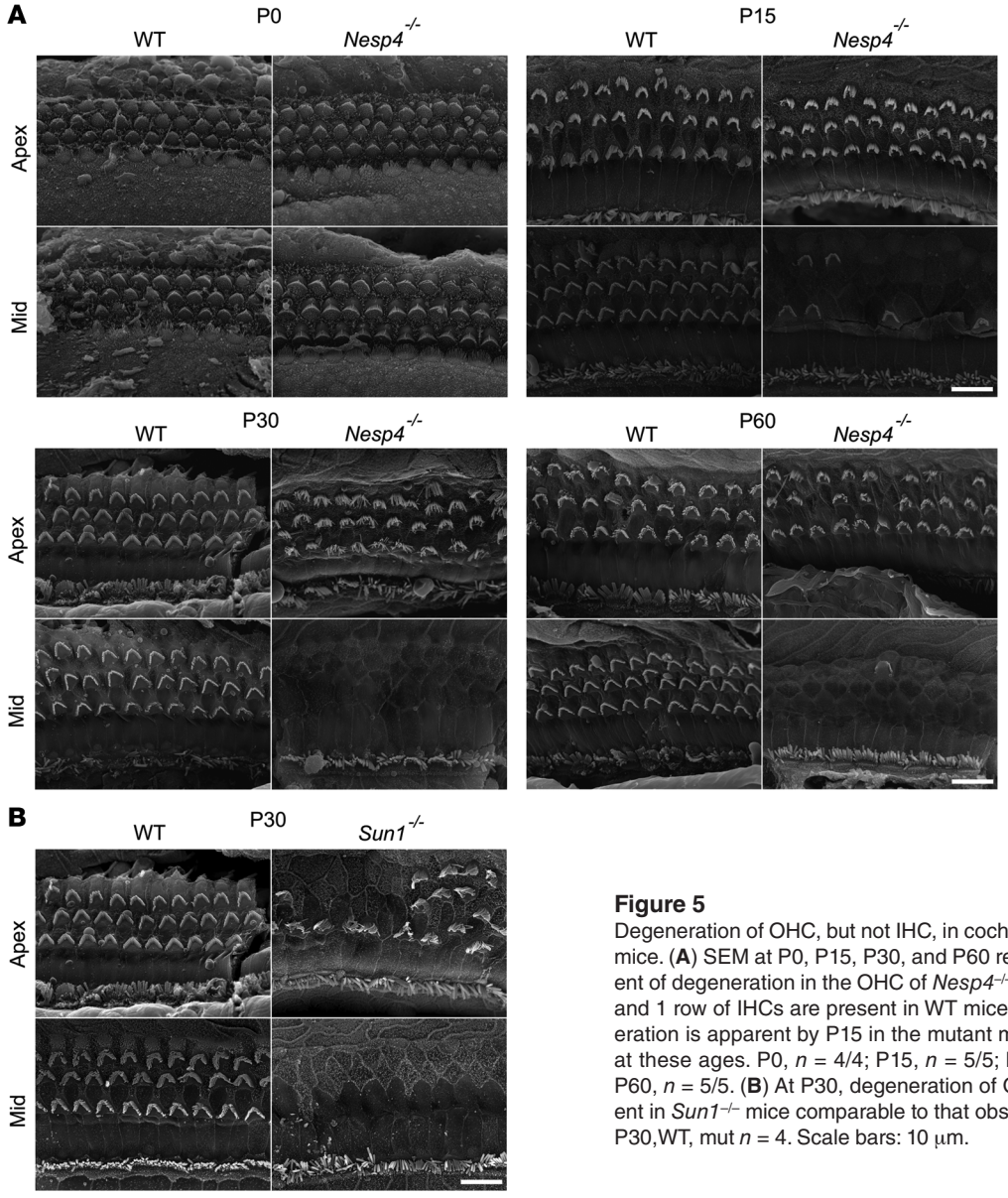

Figure 5
Degeneration of OHC, but not IHC, in cochlea of *Nesp4*$^{-/-}$ and *Sun1*$^{-/-}$ mice. (**A**) SEM at P0, P15, P30, and P60 reveals a mid to apical gradient of degeneration in the OHC of *Nesp4*$^{-/-}$ mice. Three rows of OHCs and 1 row of IHCs are present in WT mice, whereas the OHC degeneration is apparent by P15 in the mutant mice. The IHC remain intact at these ages. P0, n = 4/4; P15, n = 5/5; P30, n = 5/5; P45, n = 4/4; P60, n = 5/5. (**B**) At P30, degeneration of OHC, but not IHC, is apparent in *Sun1*$^{-/-}$ mice comparable to that observed in the *Nesp4*$^{-/-}$ mice. P30,WT, mut n = 4. Scale bars: 10 μm.

nesprin-4 from the NE of hair cells and should therefore exhibit a pattern of hearing loss similar to that observed in *Nesp4*$^{-/-}$ animals. Indeed, *Sun1*$^{-/-}$ mice were found to be deaf, with changes in hair cell morphology that bore a striking resemblance to those seen in the *Nesp4*$^{-/-}$ mice. In both mutants, the nuclei in OHCs, the auditory cells most affected by the loss of these 2 LINC complex proteins, showed a dramatic repositioning from a basal to apical location.

Nuclear repositioning is an essential component of cell differentiation and development and occurs in cells including neurons, epithelial cells, and myocytes. For example, it is a necessary and dynamic process in oogenesis and embryogenesis of *Drosophila* (18). Not only do nuclei migrate through the cell, but once achieving their ideal location, they require an anchor in order not to float or move from their designated locale. The positioning is facilitated by components of the cytoskeleton, including microtubules, kinesins, and dyneins (18).

In the cochlea, OHCs are considered to be the amplifiers of sound, while IHCs are the primary sensory cells (19). A property of OHCs is their motile nature, since their length changes as a result of membrane hyperpolarization and depolarization (4). OHCs possess at least 2 types of motility that are broadly characterized as fast and slow. The fast motile response, also known as electromotility, is ATP independent and prestin mediated and is responsible for the cochlear amplification properties of OHCs (reviewed in refs. 4, 20, 21). Slow motile responses, on the other hand, are mediated by efferent innervations, require ATP, and alter OHC properties, such as axial stiffness and length, in part through modification of cytoskeletal proteins (20, 22, 23). Slow motility is thought to be important for tuning the OHCs to large decibel variations in sound input, optimizing their cochlear amplification role, and also preventing potential overstimulation that can result in cellular damage and cell death (ref. 24 and reviewed in ref. 25). An aberrantly positioned nucleus might

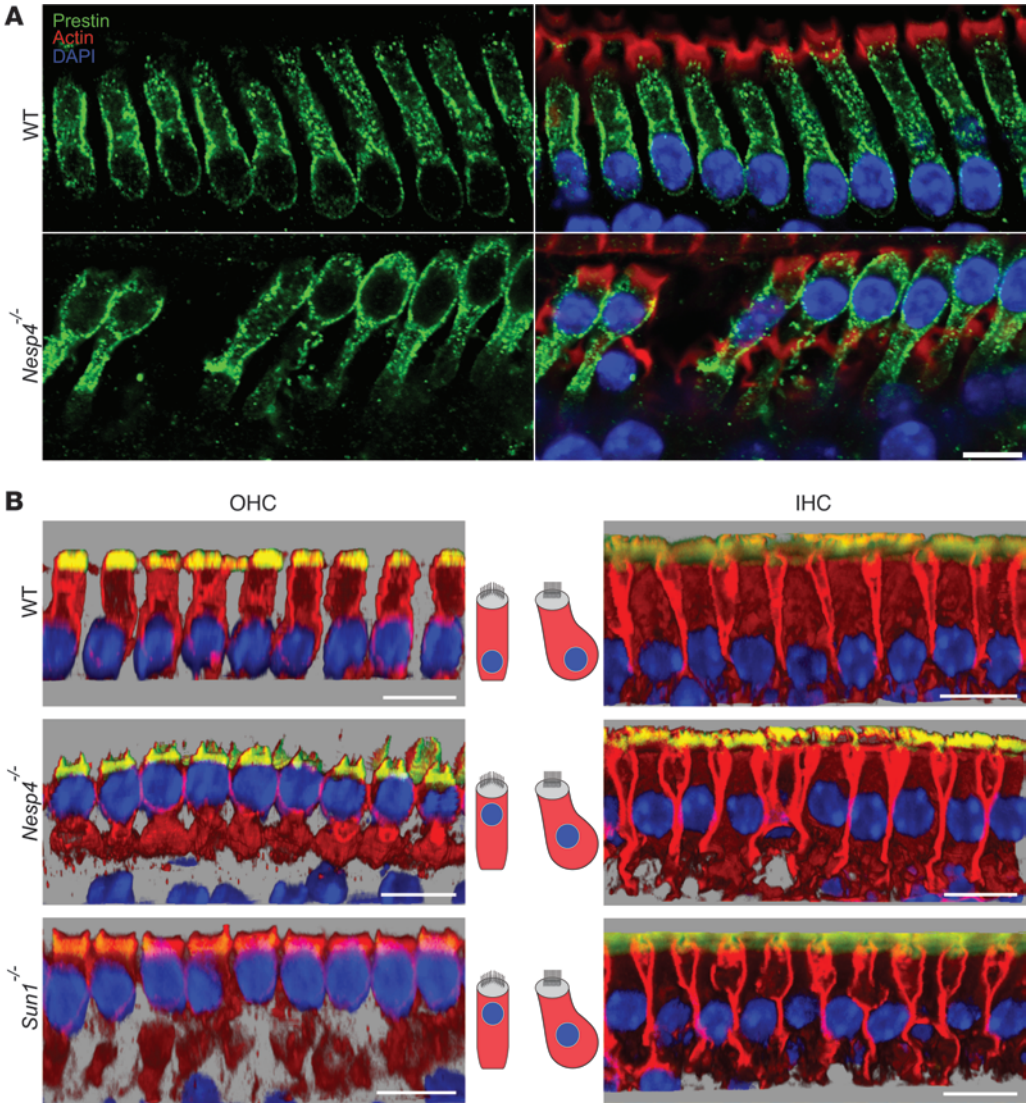

Figure 6
Nuclear localization of hair cells in *Nesp4*$^{-/-}$ and *Sun1*$^{-/-}$ mice. (**A**) Whole-mount preparations of cochlea at P14 demonstrate the position of the nuclei at the base of WT OHCs. In contrast, the nuclei appear toward the apical surface of the cells in *Nesp4*$^{-/-}$ OHCs. Prestin labels the OHC membrane (green), with phalloidin-labeling actin concentrated in the stereocilia (red) and DAPI staining the nuclei (blue). (**B**) Nuclear mislocalization of OHCs can be observed by 3D analysis of confocal stacks using Imaris software. Cochlea whole-mount preparations from WT, *Nesp4*$^{-/-}$, and *Sun1*$^{-/-}$ mice were immunostained with Na^+/K^+ ATPase to label the cytoplasmic membrane (red), phalloidin to label the actin concentrated in the stereocilia (yellow), and DAPI to stain the nuclei (blue). Note location of the nuclei at the base of OHCs derived from WT mice and location of the nuclei at the apex in mutant mice. The nuclei of the IHCs have changed their position slightly. Scale bars: 15 μm.

compromise the ability of OHCs to undergo electromotility, which would inhibit cochlear amplification and may eventually stress the OHCs, causing them to die. Alternatively, rearrangement of the cytoskeleton due to an apical shift in the position of the nucleus may then render the OHCs incapable of slow motility and more susceptible to mechanical damage, ultimately leading to apoptosis.

Although the precise position of nuclei in mammalian hair cells during development has not been systematically looked at, we observed that OHC nuclei are localized in the base of this elongated cell (Figure 6). In contrast, in *Nesp4*$^{-/-}$ and *Sun1*$^{-/-}$ OHC, the nuclei lose their polarized position in the cell and move toward the apex. While the anchor for the basal positioning in OHC is unknown, in HEK293 cells, nesprin-4 binds to a conventional kinesin-1, Kif5b, and plays an essential role in microtubule-dependent nuclear positioning (6). Kinesins are mostly plus-end–directed microtubule motor proteins that facilitate vesicle transport along microtubules (26). In other epithelial cell types, microtubule bundles are aligned with the long axis of the cell and extend from the apical to basal plasma membrane domains. The orientation of these bundles is such that the microtubule minus ends are positioned predominantly at the cell apex (27). The cytoplasmic microtubule network in OHCs also appears to originate at the apex of the cell and seems to conform to this general epithelial scheme (28, 29). Therefore, we would predict that loss of nesprin-4, and hence kinesin-1, from the cytoplasmic face of the NE, should result in an

untethering of the nucleus from the microtubule cytoskeleton and a subsequent inability to efficiently localize the nucleus to the base of the cell, which is precisely what we observed.

Progressive damage of OHCs was observed beginning at P15 in the *Nesp4*$^{-/-}$ mice (Figure 5), while IHC disruption was only observed at P180 (data not shown). While the IHCs were lost much later than the OHCs, our ABR results from various ages (P15-P60) imply that the IHCs were functionally affected by the loss of the LINC complex much earlier. The change in nuclear position was minor compared with that seen in the OHCs. The fact that this did not result in IHC death at the same rate as OHC death is likely a direct reflection of the physiological and functional differences between the two. The loss of IHCs at a later age could be directly due to the loss of the LINC complex in IHCs or could be a secondary effect. Secondary IHC loss, following primary OHC damage, was previously reported in mice with a targeted disruption of prestin, an OHC-specific protein, and acoustic injuries (30, 31). This subsequent IHC loss might explain the more severe hearing loss observed in the affected DFNB76 family members, as well as the *Nesp4*$^{-/-}$ mice, compared with that expected for hearing impairment associated only with loss of OHC.

Comparison of the morphology of hair cell bundles from *Nesp4*$^{-/-}$ and *Sun1*$^{-/-}$ mice highlights the same pattern of OHC loss that progresses from the base to the apex. As was the case in the *Nesp4*$^{-/-}$ mice, maturation of the OHCs in *Sun1*$^{-/-}$ mice was accompanied by mislocalization of the OHC nuclei from basal to apical regions of the cells. This striking similarity between the *Sun1*$^{-/-}$ and *Nesp4*$^{-/-}$ phenotype in the mouse ear provides compelling evidence that a nesprin-4–Sun1 LINC complex has an essential role in OHC morphogenesis and viability. Therefore, LINC complex dysfunction most likely underlies the pathology of *SYNE4* mutation–associated hearing loss in humans.

Nesprins are known to be involved in human disease. For example, mutations in *SYNE1*, which encodes a protein expressed mainly in the cerebellum, have been implicated in autosomal recessive cerebellar ataxia (32). Mutations in the same gene are predicted to lead to an autosomal recessive form of myogenic arthrogryposis multiplex congenita (AMC) (33). Emery-Dreifuss muscular dystrophy-5 (EDMD5) patients, with late onset neuromuscular disorders, harbor mutations in both *SYNE1* and *SYNE2* (34). Clearly these proteins, responsible for anchoring myonuclei under neuromuscular junctions and therefore coupling the nucleoskeleton to the cytoskeleton, are required for maintaining the structure of the LINC complex. A similar mechanism appears to be responsible for deafness due to *SYNE4* mutations.

Exon skipping, such as what we observe in the human *SYNE4* mutations, was previously reported in human disease such as early-onset severe retinal dystrophy (EOSRD) and dystrophinopathies (35). The c.228delAT mutation creates an hnRNPA1 binding site (AGATGGT→AGGGT), involved in splicing (36) and potentially explains the cause of the exon skipping in these families. In transfected cells, we demonstrate that both variants, with and without exon 2, result in stop codons and truncated proteins of 93 and 51 amino acids, respectively. Although they are much shorter than the full-length 404–amino acid protein, these proteins appear to be expressed in transfected cells (Figure 2). The phenomenon of exon skipping, leading to a nonsense mutation, has been described as a rescue mechanism, enabling the resulting protein to function partially and in doing so, replacing a drastic phenotype by a milder one. The high-tone hearing loss could be characterized as a milder loss relative to the more drastic hearing loss observed in the *Nesp4*$^{-/-}$ mice. However, the predicted mRNA is more likely to undergo nonsense-mediated decay (NMD) and even if translated, result in a protein lacking the spectrin repeat or kinesin binding domain of nesprin-4. In all likelihood the c.228delAT mutation represents a functional deletion of the *SYNE4* gene.

We have described, for what we believe is the first time, a mutation in a gene encoding a LINC complex protein resulting in deafness. This reveals yet another piece of the intricate puzzle that characterizes genetic heterogeneity of deafness, with a multitude of proteins involved in this sensory disease. Most compelling, each genetic mutation reveals an entirely new mechanism for the pathophysiology of deafness. Overall, our observations demonstrate a critical role for nuclear positioning in sensory hair cells, a fundamental criterion for normally functioning cells, and link nesprin-4 and Sun1 to this phenomenon. A pathomechanism for impaired auditory function, with a defective LINC complex, implicates this pathway in the mammalian inner ear. These findings further suggest that defects in other components of the intimately linked protein network of the NE/lamina may be found to result in forms of hearing loss. We predict that mutations in *SUN1* linked to human deafness may be discovered using massively parallel sequencing in future screens.

Methods

Clinical evaluation. Family members provided hearing assessments, pedigree information, and whole blood from which DNA was extracted and, for some, lymphoblast cell lines developed. Pure tone audiometry was performed by standard methods (37).

Linkage and homozygosity mapping and Sanger sequencing. Genome-wide linkage analysis was performed at the Institute of Life Sciences, Hebrew University (Jerusalem, Israel) on an ABI3700 automated DNA analyzer using 350 microsatellite markers from the MDC-Genethon database (38). Sizing and genotyping were performed using GENESCAN and GENOTYPER (Applied Biosystems). Candidate genes were Sanger sequenced from genomic DNA using standard methods.

Massively parallel sequencing. Genomic regions harboring 284 genes were captured by hybridization of complementary custom-designed biotinylated cRNA oligonucleotides, then analyzed with paired-end sequencing on an Illumina HiSeq2000 instrument, as reported previously (11). In the current experiment, the final capture design targeting 4475 exons from 284 genes was 1.86 Mb (Supplemental Table 1; supplemental material available online with this article; doi:10.1172/JCI66911DS1). Median base coverage ranged from 113-641x, with coverage of 84% of targeted base pairs at 10 reads per base and 73% of targeted base pairs at 30 reads.

Generation and maintenance of mutant mice. To create the *Nesp4*$^{-/-}$ mice, an *IRES*–β-*gal* neomycin selectable cassette (*PgkNeo*) flanked by loxP sites was inserted into the *Nesp4* gene using *Eco*RI and *Spe*I sites, resulting in deletion of part of exon 1 and all of exons 2–6. The targeting vector was linearized and electroporated into Bruce4 ES cells that were largely of C57BL/6 origin. Clones selected with neomycin were picked, expanded, and screened for recombination. Two recombinant ES lines were injected into C57BL/6$^{cBrd/cBrd/Cr}$ blastocysts, and chimaeras were bred to produce germline offspring as described (39). Homozygous, heterozygous, and WT mice were distinguished by PCR using the following sets of primers: WT_F 5′ ACTCCCAGCTCCAAGCTACA, WT_R 5′ GCAGAGCCAAAGAAACCAAG to probe for the WT allele, LacZ_F 5′ GTCTCGTTGCTGCATAAACC, and LacZ_R 5′ TCGTCTGCTCATCCATGACC to probe for the galactosidase gene. Tails were processed by alkaline lysis and DNA was PCR amplified using MangoMix (Bioline). Heterozygous mice were intercrossed to obtain homozygous mutant mice. *Sun1*$^{-/-}$ and *Sun2*$^{-/-}$ mice were maintained and genotyped as described (15).

qRT-PCR analysis. For salivary gland, tissue was snap-frozen in liquid nitrogen and homogenized using lysing matrix D in a MP FastPrep-24 tissue homogenizer in RNABle (Eurobio) followed by chloroform extraction and ethanol precipitation. Samples were further purified using the RNeasy Mini Kit (QIAGEN). cDNA was generated using Thermoscript reverse transcriptase (Invitrogen), and qRT-PCR was carried out on a 7500 Fast Real-Time PCR system using Fast SYBR Green Master Mix (Applied Biosystems). Cochlea were frozen in liquid nitrogen. RNA was extracted using the RNeasy Plus Mini Kit (QIAGEN) followed by conversion to cDNA using the High Capacity cDNA Reverse Transcription Kit (Applied Biosystems). SYBR Green with cyclophilin as a control was used or the TaqMan Gene Expression Assay (Applied Biosystems) together with FastStart Universal Probe Master Mix (Roche) on a 7900 Fast Real-Time PCR with TBP as a control. For every time point, at least 3 mice were analyzed in triplicate.

Cell culture and transfection. COS-7 cells were grown in DMEM containing 10% FBS and antibiotics (Beit Haemek Biological Industries) at 37°C with 5% CO_2. The following plasmids were transfected using Lipofectamine 2000 (Invitrogen) according to the manufacturer's instructions: pcDNA-Nesp4-GFP, pcDNA-Nesp4-GFP containing the human c.228delAT mutation, and pcDNA-Nesp4-GFP lacking exon 2. The cells were harvested in cold PBS 48 hours after transfection.

Western blot analysis. For cochlea, NP40 was used for lysis followed by 30 second sonication on ice. Protein concentration for each sample was determined using Bradford assay (Sigma-Aldrich), and 100 μg of total protein were loaded on 8% SDS polyacrylamide gels (SDS-PAGE) and then transferred to PVDF membrane (Millipore). Rabbit anti-GFP (Invitrogen) was used as primary antibody and HRP-conjugated goat anti-rabbit (Jackson Laboratories) as secondary antibody. Signal was generated using SuperSignal West Pico Chemiluminescent Substrate (Thermo Scientific) and detected on SuperRX films (Fujifilm). For salivary gland, equal fractions of the submandibular salivary gland were isolated from WT and *Nesp4*$^{-/-}$ mice, snap-frozen in liquid nitrogen, and lysed directly into 2× sample buffer. Equal volumes were resolved by SDS-PAGE, transferred to PVDF membrane, probed with rabbit anti–nesprin-4 primary antibody and HRP-conjugated donkey anti-rabbit (GE Healthcare) secondary antibody, and visualized as above.

Immunolocalization. Expression of nesprin-4, Sun1, prestin, and sodium potassium ATPase were evaluated by whole-mount immunofluorescence in inner ears from indicated ages. Inner ears were dissected and fixed overnight using 4% paraformaldehyde, and fine dissection was conducted to expose the sensory epithelia. Samples were treated with 0.2% Triton X-100 in PBS for 1 hour followed by 1 hour incubation in blocking buffer (10% normal donkey serum in 0.2% Triton X-100 PBS). Primary antibodies were diluted in blocking buffer and incubated with the samples overnight at 4°C. Antibodies used were as follows: rabbit anti–nesprin-4 (GST-Nesp4 [aa 1–90] fusion protein; Rockland Immunochemicals) (6), rabbit anti-Sun1 (gift from Chi Ya-Hui, National Health Research Institutes, Taiwan), goat anti-prestin (C-16, 1:100; Santa Cruz Biotechnology Inc.), and rabbit mAb anti-sodium potassium ATPase (1:100; Abcam). After washes in 0.2% Triton X-100 PBS, samples were incubated in secondary antibody (diluted in blocking buffer) for 1 hour at room temperature. The following secondary reagents were used: donkey anti-goat Alexa Fluor 488, donkey anti-mouse Alexa Fluor 568, donkey anti-rabbit Alexa Fluor 488, donkey anti-rabbit Alexa Fluor 594, and phalloidin Alexa Fluor 647 (Invitrogen). Samples were washed in 0.2% Triton X-100 followed by several washes in PBS only and mounted in ProLong Gold antifade mounting medium (Invitrogen). Imaging was done with the LSM 510 confocal microscope (Zeiss). Postacquisition processing of confocal stacks was performed using Imaris software (Bitplane AG). Stacks were cropped in 3D and rendered using "blend" visualization; the proximal row of OHC was exposed using clipping planes.

SEM. Inner ears from mice at P0, P15, P30, and P60 were dissected and fixed overnight using 2% glutaraldehyde solution. The samples were then fine dissected, and incubated with osmium and tetroxide-thiocarbohydrazide alternately according to the OTOTO protocol, described previously (40). After ethanol dehydration, the samples were processed using critical point drying followed by gold-coating procedure and were scanned using a JSM 840A Scanning Electron Microscope (Jeol).

ABR testing. Mice of different ages (P15, P30, P60) were anesthetized by i.p. injection of Avertin (0.015 ml/g mouse) and placed on a heating pad in an acoustic chamber (MAC-1; Industrial Acoustic Company). For hearing threshold evaluation, 3 subdermal electrodes, ground, reference, and active, were placed at the mouse head behind the left ear, behind the right ear, and on the forehead, respectively. TDT software (Biosig RZ) and hardware (RZ and MF1 speakers) were used, with speakers placed 10 cm in front of the mouse. Speakers were calibrated using an ACO Pacific 7017 microphone. Two protocols were used: click stimuli, in which the mouse was presented with a wide spectrum click (0.1 ms) in increasing levels, ranging between 10 dB and 90 dB in 5-dB steps, and tone burst stimuli of 6 single frequencies (1 ms), including 6 kHz, 12 kHz, 18 kHz, 24 kHz, 30 kHz, and 36 kHz in increasing levels between 10 dB and 90 dB in 5-dB steps. Each point of measurement was recorded and averaged 512 times and analyzed; threshold was determined as the lowest recognizable ABR response.

Behavioral testing. The general behavior and vestibular function of 6 *Nesp4* mutant mice was compared with the WT behavior of 6 littermates using several tests, performed on an empty large platform that was thoroughly cleaned between mice. These tests reflect the ability of the mice to sense gravity and perceive its sense of balance. Mice were given 2 minutes to adjust, followed by 2–3 minutes in which their general behavior was tested using the modified SHIRPA protocol (12). Reaching response and circling and head-bobbing behavior were evaluated as previously described (41).

Statistics. Student's 2-tailed *t* test *P* values of less than 0.05 were considered to be statistically significant and those of less than 0.005 were considered to be highly statistically significant. The data in the figures are presented by mean ± SEM.

Study approval. The study was approved by the Helsinki Committee of Tel Aviv University and the National Helsinki Committee for Human Genetic Research of the Israel Ministry of Health. Family members provided informed consent. All procedures involving animals met NIH guidelines and were approved by the Animal Care and Use Committees of Tel Aviv University and A*STAR.

Acknowledgments

The authors thank the families for their participation in this study. This research was funded by the NIH (National Institute on Deafness and Other Communication Disorders) (R01DC011835), I-CORE Gene Regulation in Complex Human Disease, Center No. 41/11, and the Hedrich Charitable Trust (to K.B. Avraham); and the Singapore Biomedical Research Council and the Singapore Agency for Science, Technology and Research (A*STAR) (to B. Burke and C.L. Stewart). We also wish to thank Yosef Gruenbaum, Mary-Claire King, Gil Ast, and Dror Hollander for helpful discussions, and Varda Oron-Karni and Nitzan Kol for massively parallel sequencing.

Received for publication September 25, 2012, and accepted in revised form November 29, 2012.

Address correspondence to: Karen B. Avraham, Department of Human Molecular Genetics and Biochemistry, Sackler Faculty of Medicine, Tel Aviv University, Tel Aviv 69978, Israel. Phone: 972.3.640.6642; Fax: 972.3.640.9360; E-mail: karena@post.tau.ac.il.

1. Morton CC, Nance WE. Newborn hearing screening — a silent revolution. *N Engl J Med*. 2006; 354(20):2151–2164.
2. Brownstein Z, Bhonker Y, Avraham KB. High-throughput sequencing to decipher the genetic heterogeneity of deafness. *Genome Biol*. 2012;13(5):245.
3. Petit C, Levilliers J, Hardelin JP. Molecular genetics of hearing loss. *Annu Rev Genet*. 2001;35:589–646.
4. Dallos P. Cochlear amplification, outer hair cells and prestin. *Curr Opin Neurobiol*. 2008;18(4):370–376.
5. Burke B. It takes KASH to hitch to the SUN. *Cell*. 2012;149(5):961–963.
6. Roux KJ, et al. Nesprin 4 is an outer nuclear membrane protein that can induce kinesin-mediated cell polarization. *Proc Natl Acad Sci U S A*. 2009;106(7):2194–2199.
7. Starr DA, Fischer JA. KASH 'n Karry: the KASH domain family of cargo-specific cytoskeletal adaptor proteins. *Bioessays*. 2005;27(11):1136–1146.
8. Crisp M, et al. Coupling of the nucleus and cytoplasm: role of the LINC complex. *J Cell Biol*. 2006;172(1):41–53.
9. Burke B, Stewart CL. Life at the edge: the nuclear envelope and human disease. *Nat Rev Mol Cell Biol*. 2002;3(8):575–585.
10. Burke B, Stewart CL. The laminopathies: the functional architecture of the nucleus and its contribution to disease. *Annu Rev Genomics Hum Genet*. 2006;7:369–405.
11. Brownstein Z, et al. Targeted genomic capture and massively parallel sequencing to identify genes for hereditary hearing loss in Middle Eastern families. *Genome Biology*. 2011;12(9):R89.
12. Green EC, Gkoutos GV, Lad HV, Blake A, Weekes J, Hancock JM. EMPReSS: European mouse phenotyping resource for standardized screens. *Bioinformatics*. 2005;21(12):2930–2931.
13. Chi YH, et al. Requirement for Sun1 in the expression of meiotic reproductive genes and piRNA. *Development*. 2009;136(6):965–973.
14. Ding X, Xu R, Yu J, Xu T, Zhuang Y, Han M. SUN1 is required for telomere attachment to nuclear envelope and gametogenesis in mice. *Dev Cell*. 2007;12(6):863–872.
15. Lei K, et al. SUN1 and SUN2 play critical but partially redundant roles in anchoring nuclei in skeletal muscle cells in mice. *Proc Natl Acad Sci U S A*. 2009;106(25):10207–10212.
16. Pujol R, Zajic G, Dulon D, Raphael Y, Altschuler RA, Schacht J. First appearance and development of motile properties in outer hair cells isolated from guinea-pig cochlea. *Hear Res*. 1991;57(1):129–141.
17. Sosa BA, Rothballer A, Kutay U, Schwartz TU. LINC complexes form by binding of three KASH peptides to domain interfaces of trimeric SUN proteins. *Cell*. 2012;149(5):1035–1047.
18. Starr DA, Han M. ANChors away: an actin based mechanism of nuclear positioning. *J Cell Sci*. 2003;116(pt 2):211–216.
19. Richardson GP, de Monvel JB, Petit C. How the genetics of deafness illuminates auditory physiology. *Annu Rev Physiol*. 2011;73:311–334.
20. Elgoyhen AB, Franchini LF. Prestin and the cholinergic receptor of hair cells: positively-selected proteins in mammals. *Hear Res*. 2011;273(1-2):100–108.
21. Ashmore J. Cochlear outer hair cell motility. *Physiol Rev*. 2008;88(1):173–210.
22. Dallos P, et al. Prestin-based outer hair cell motility is necessary for mammalian cochlear amplification. *Neuron*. 2008;58(3):333–339.
23. Sziklai I, Szonyi M, Dallos P. Phosphorylation mediates the influence of acetylcholine upon outer hair cell electromotility. *Acta Otolaryngol*. 2001; 121(2):153–156.
24. Frolenkov GI, Mammano F, Kachar B. Regulation of outer hair cell cytoskeletal stiffness by intracellular Ca^{2+}: underlying mechanism and implications for cochlear mechanics. *Cell Calcium*. 2003;33(3):185–195.
25. Guinan JJ Jr, Salt A, Cheatham MA. Progress in cochlear physiology after Békésy. *Hear Res*. 2012;293(1–2):12–20.
26. Lodish H, Berk A, Zipursky SL, Matsudaira P, Baltimore D, Darnell J. *Molecular Cell Biology*. 4th ed. New York, New York, USA: W.H. Freeman; 2000.
27. Bacallao R, Antony C, Dotti C, Karsenti E, Stelzer EH, Simons K. The subcellular organization of Madin-Darby canine kidney cells during the formation of a polarized epithelium. *J Cell Biol*. 1989;109(6 pt 1):2817–2832.
28. Hallworth R, McCoy M, Polan-Curtain J. Tubulin expression in the developing and adult gerbil organ of Corti. *Hear Res*. 2000;139(1–2):31–41.
29. Steyger PS, Furness DN, Hackney CM, Richardson GP. Tubulin and microtubules in cochlear hair cells: comparative immunocytochemistry and ultrastructure. *Hear Res*. 1989;42(1):1–16.
30. Liberman MC, Gao J, He DZ, Wu X, Jia S, Zuo J. Prestin is required for electromotility of the outer hair cell and for the cochlear amplifier. *Nature*. 2002;419(6904):300–304.
31. Bohne BA, Rabbitt KD. Holes in the reticular lamina after noise exposure: implication for continuing damage in the organ of Corti. *Hear Res*. 1983;11(1):41–53.
32. Gros-Louis F, et al. Mutations in *SYNE1* lead to a newly discovered form of autosomal recessive cerebellar ataxia. *Nat Genet*. 2007;39(1):80–85.
33. Attali R, et al. Mutation of *SYNE-1*, encoding an essential component of the nuclear lamina, is responsible for autosomal recessive arthrogryposis. *Hum Mol Genet*. 2009;18(18):3462–3469.
34. Zhang Q, et al. Nesprin-1 and -2 are involved in the pathogenesis of Emery Dreifuss muscular dystrophy and are critical for nuclear envelope integrity. *Hum Mol Genet*. 2007;16(23):2816–2833.
35. Nishiyama A, et al. Dystrophin nonsense mutations can generate alternative rescue transcripts in lymphocytes. *Ann Hum Genet*. 2008;72(pt 6):717–724.
36. Burd CG, Dreyfuss G. RNA binding specificity of hnRNP A1: significance of hnRNP A1 high-affinity binding sites in pre-mRNA splicing. *EMBO J*. 1994; 13(5):1197–1204.
37. [No authors listed]. Guidelines for screening for hearing impairment and middle ear disorders. *ASHA Suppl*. 1989;31(1):71–77.
38. Dib C, et al. A comprehensive genetic map of the human genome based on 5,264 microsatellites. *Nature*. 1996;380(6570):152–154.
39. Kontgen F, Stewart CL. Simple screening procedure to detect gene targeting events in embryonic stem cells. *Methods Enzymol*. 1993;225:878–890.
40. Self T, Mahony M, Fleming J, Walsh J, Brown SD, Steel KP. Shaker-1 mutations reveal roles for myosin VIIA in both development and function of cochlear hair cells. *Development*. 1998;125(4):557–566.
41. Lenz DR, Dror AA, Wekselman G, Fuchs H, de Angelis MH, Avraham KB. The inner ear phenotype of Volchok (*Vlk*): An ENU-induced mouse model for CHARGE syndrome. *Audiol Med*. 2010; 8(3):110–119.